PHYSICAL REVIEW B **96**, 161403(R) (2017)

Nonlocal Andreev entanglements and triplet correlations in graphene with spin-orbit coupling

Razieh Beiranvand,[1] Hossein Hamzehpour,[1,2] and Mohammad Alidoust[1]
[1]*Department of Physics, K.N. Toosi University of Technology, Tehran 15875-4416, Iran*
[2]*School of Physics, Institute for Research in Fundamental Sciences (IPM), 19395-5531 Tehran, Iran*

(Received 27 February 2017; published 4 October 2017)

Using a wave function Dirac Bogoliubov–de Gennes method, we demonstrate that the tunable Fermi level of a graphene layer in the presence of Rashba spin-orbit coupling (RSOC) allows for producing an anomalous nonlocal Andreev reflection and equal spin superconducting triplet pairing. We consider a graphene nanojunction of a ferromagnet-RSOC-superconductor-ferromagnet configuration and study scattering processes, the appearance of spin triplet correlations, and charge conductance in this structure. We show that the anomalous crossed Andreev reflection is linked to the equal spin triplet pairing. Moreover, by calculating current cross-correlations, our results reveal that this phenomenon causes negative charge conductance at weak voltages and can be revealed in a spectroscopy experiment, and may provide a tool for detecting the entanglement of the equal spin superconducting pair correlations in hybrid structures.

DOI: 10.1103/PhysRevB.96.161403

Introduction. Superconductivity and its hybrid structures with other phases can host a wide variety of intriguing fundamental phenomena and functional applications such as Higgs mechanism [1], Majorana fermions [2], topological quantum computation [3], spintronics [4], and quantum entanglement [5–8]. The quantum entanglement describes quantum states of correlated objects with nonzero distances [6,8] that are expected to be employed in novel ultrafast technologies such as secure quantum computing [3,6].

From the perspective of BCS theory, s-wave singlet superconductivity is a bosonic phase created by the coupling of two charged particles with opposite spins and momenta (forming a so-called Cooper pair) through an attractive potential [9]. The two particles forming a Cooper pair can spatially have a distance equal or less than a coherence length ξ_S [9]. Therefore, a Cooper pair in the BCS scenario can serve as a natural source of entanglement with entangled spin and momentum. As a consequence, one can imagine a heterostructure made of a single s-wave superconductor and multiple nonsuperconducting electrodes in which an electron and hole excitation from different electrodes are coupled by means of a nonlocal Andreev process [7,10–13]. This idea has so far motivated numerous theoretical and experimental endeavours to explore this entangled state in various geometries and materials [12,14–27]. Nonetheless, the nonlocal Andreev process is accompanied by an elastic cotunneling current that makes it practically difficult to detect unambiguously the signatures of a nonlocal entangled state [10,11,13–17]. This issue, however, may be eliminated by making use of a graphene-based hybrid device that allows for locally controlled Fermi level [26].

On the other hand, the interplay of s-wave superconductivity and an inhomogeneous magnetization can convert the superconducting spin singlet correlations into equal spin triplets [28,29]. After the theoretical prediction of the spin triplet superconducting correlations much effort has been made to confirm their existence [4,30–43]. For example, a finite supercurrent was observed in a half-metallic junction that was attributed to the generation of equal spin triplet correlations near the superconductor–half-metal interface [30]. Also, it was observed that in a Josephson junction made of a holmium–cobalt–holmium stack, the supercurrent as a function of the cobalt layer decays exponentially without any sign reversals due to the presence of equal spin triplet pairings [36,37]. One more signature of the equal spin triplet pairings generated in the hybrid structures may be detected in superconducting critical temperature [43–46] and density of states [47–50]. Nevertheless, a direct observation of the equal spin triplet pairings in the hybrid structures is still lacking.

In this Rapid Communication, we show that the existence of the equal spin superconducting triplet correlations can be revealed through charge conductance spectroscopy of a graphene-based ferromagnet–Rashba SOC–superconductor–ferromagnet junction. We study all possible electron/hole reflections and transmissions in such a configuration and show that by tuning the Fermi level a regime is accessible in which spin reversed cotunneling and usual crossed Andreev reflections are blocked while a conventional cotunneling and anomalous nonlocal Andreev channel is allowed. We justify our findings by analyzing the band structure of the system. Moreover, we calculate various superconducting correlations and show that, in this regime, the equal spin triplet correlation has a finite amplitude while the unequal spin triplet component vanishes. Our results show that the anomalous crossed Andreev reflection results in a negative charge conductance at low voltages applied across the junction and can be interpreted as evidence for the generation and entanglement of equal spin superconducting triplet correlations in hybrid structures [51–55].

Method and results. As seen in Fig. 1, we assume that the ferromagnetism, superconductivity, and spin-orbit coupling are separately induced into the graphene layer through the proximity effect as reported experimentally in Refs. [56–58] for isolated samples. Therefore, the low-energy behavior of quasiparticles, quantum transport characteristics, and thermodynamics of such a system can be described by the Dirac Bogoliubov–de Gennes (DBdG) formalism [34,59]:

$$\begin{pmatrix} \mathcal{H}_{\rm D} + \mathcal{H}_i - \mu^i & \Delta e^{i\phi} \\ \Delta^* e^{-i\phi} & \mu^i - \mathcal{T}[\mathcal{H}_{\rm D} - \mathcal{H}_i]\mathcal{T}^{-1} \end{pmatrix} \begin{pmatrix} u \\ v \end{pmatrix} = \varepsilon \begin{pmatrix} u \\ v \end{pmatrix}, \tag{1}$$

in which ε is the quasiparticles' energy and $\mathcal{T}$ represents a time-reversal operator [34,59]. Here $\mathcal{H}_{\rm D} = \hbar v_F s_0 \otimes (\sigma_x k_x + \sigma_y k_y)$ with v_F being the Fermi velocity [59]. $s_{x,y,z}$ and $\sigma_{x,y,z}$ are 2×2 Pauli matrices, acting on the spin and pseudospin degrees of freedom, respectively. The superconductor region with a macroscopic phase ϕ is described by a gap Δ in the energy spectrum. The chemical potential in a region i is shown by μ^i while the corresponding Hamiltonians read

$$\mathcal{H}_i = \begin{cases} \mathcal{H}_{\rm F} = h_l(s_z \otimes \sigma_0), & x \leqslant 0 \\ \mathcal{H}_{\rm RSO} = \lambda(s_y \otimes \sigma_x - s_x \otimes \sigma_y), & 0 \leqslant x \leqslant L_{\rm RSO} \\ \mathcal{H}_{\rm S} = -U_0(s_0 \otimes \sigma_0), & L_{\rm RSO} \leqslant x \leqslant L_{\rm S} + L_{\rm RSO} \\ \mathcal{H}_{\rm F} = h_r(s_z \otimes \sigma_0), & L_{\rm S} + L_{\rm RSO} \leqslant x. \end{cases} \tag{2}$$

The magnetization $\vec{h}_{l,r}$ in the ferromagnet segments are assumed fixed along the z direction with a finite intensity $h_{l,r}$. λ is the strength of Rashba spin-orbit coupling and U_0 is an electrostatic potential in the superconducting region. Previous self-consistent calculations have demonstrated that sharp interfaces between the regions can be an appropriate approximation [34,59–62]. The length of the RSO and S regions are $L_{\rm RSO}$ and $L_{\rm S}$, respectively.

To determine the properties of the system, we diagonalize the DBdG Hamiltonian equation (1) in each region and obtain corresponding eigenvalues:

$$\varepsilon = \begin{cases} \pm\mu^{\rm F_l} \pm \sqrt{\left(k_x^{\rm F_l}\right)^2 + q_n^2} \pm h_l, & x \leqslant 0 \\ \pm\mu^{\rm RSO} \pm \sqrt{\left(k_x^{\rm RSO}\right)^2 + q_n^2 + \lambda^2 \pm \lambda}, & 0 \leqslant x \leqslant L_{\rm RSO} \\ \pm\sqrt{\left(\mu^S + U_0 \pm \sqrt{\left(k_x^S\right)^2 + q_n^2}\right)^2 + |\Delta_0|^2}, & L_{\rm RSO} \leqslant x \leqslant L_{\rm RSO} + L_{\rm S} \\ \pm\mu^{\rm F_r} \pm \sqrt{\left(k_x^{\rm F_r}\right)^2 + q_n^2} \pm h_r, & L_{\rm RSO} + L_{\rm S} \leqslant x. \end{cases} \tag{3}$$

The associated eigenfunctions are given in Ref. [63]. The wave vector of a quasiparticle in region i is $\mathbf{k}_i = (k_x^i, q_n)$ so that its transverse component is assumed conserved upon scattering. In what follows, we consider a heavily doped superconductor $U_0 \gg \varepsilon, \Delta$ which is an experimentally relevant regime [59]. We also normalize energies by the superconducting gap at zero temperature Δ_0 and lengths by the superconducting coherent length $\xi_S = \hbar v_F/\Delta_0$.

Since the magnetization in F regions is directed along the z axis, which is the quantization axis, it allows for unambiguously analyzing spin-dependent processes. Therefore, we consider a situation where an electron with spin-up (described by wave function $\psi_{e,\uparrow}^{\rm F,+}$) hits the RSO interface at $x = 0$ due to a voltage bias applied. This particle can reflect back ($\psi_{e,\uparrow(\downarrow)}^{\rm F,-}$) with probability amplitude $r_N^{\uparrow(\downarrow)}$ or enter the superconductor as a Cooper pair and a hole ($\psi_{h,\uparrow(\downarrow)}^{\rm F,-}$) with probability amplitude $r_A^{\uparrow(\downarrow)}$ reflects back, which is the so-called Andreev reflection. Hence, the total wave function in the left F region is (see Refs. [53,63])

$$\Psi^{\rm F_l}(x) = \psi_{e,\uparrow}^{\rm F,+}(x) + r_N^{\uparrow}\psi_{e,\uparrow}^{\rm F,-}(x) + r_N^{\downarrow}\psi_{e,\downarrow}^{\rm F,-}(x) + r_A^{\downarrow}\psi_{h,\downarrow}^{\rm F,-}(x) + r_A^{\uparrow}\psi_{h,\uparrow}^{\rm F,-}(x). \tag{4}$$

The total wave function in the RSO and S parts are superpositions of right- and left-moving spinors with different quantum states n; $\psi_n^{\rm RSO}$ and $\psi_n^{\rm S}$ (see Ref. [63]): $\Psi^{\rm RSO}(x) = \sum_{n=1}^{8} a_n \psi_n^{\rm RSO}(x)$ and $\Psi^{\rm S}(x) = \sum_{n=1}^{8} b_n \psi_n^{\rm S}(x)$, respectively. The incident particle eventually can transmit into the right F region as an electron or hole ($\psi_{e,\uparrow\downarrow}^{\rm F,+}, \psi_{h,\uparrow\downarrow}^{\rm F,+}$) with probability amplitudes $t_e^{\uparrow\downarrow}$ and $t_h^{\uparrow\downarrow}$:

$$\Psi^{\rm F_r}(x) = t_e^{\uparrow}\psi_{e,\uparrow}^{\rm F,+}(x) + t_e^{\downarrow}\psi_{e,\downarrow}^{\rm F,+}(x) + t_h^{\downarrow}\psi_{h,\downarrow}^{\rm F,+}(x) + t_h^{\uparrow}\psi_{h,\uparrow}^{\rm F,+}(x). \tag{5}$$

The transmitted hole is the so-called crossed Andreev reflection (CAR). By matching the wave functions at F-RSO, RSO-S, and S-F interfaces we obtain the probabilities described above. Figure 2 exhibits the probabilities of usual electron cotunneling $|t_e^{\uparrow}|^2$, spin-flipped electron $|t_e^{\downarrow}|^2$, usual crossed Andreev reflection $|t_h^{\downarrow}|^2$, and anomalous crossed Andreev reflection $|t_h^{\uparrow}|^2$. To have a strong anomalous CAR signal, we set $L_S = 0.4\xi_S$ which is smaller than the superconducting coherence length and $L_{\rm RSO} = 0.5\xi_S$ [11]. We also choose $\mu^{\rm F_l} = \mu^{\rm F_r} = h_l = h_r = 0.8\Delta_0$, $\mu^{\rm RSO} = 2.6\Delta_0$, $\lambda = \Delta_0$ and later clarify physical reasons behind this choice using band-structure analyses. In terms of realistic numbers, if the superconductor is Nb [62] with a gap of the order of $\Delta_0 \sim 1.03$ meV and coherence length $\xi_S \sim 10$ nm, the chemical potentials, magnetization strengths, and the RSO intensity are $\mu^{\rm F_l} = \mu^{\rm F_r} = h_l = h_r = 0.824$ meV, $\mu^{\rm RSO} = 2.68$ meV,

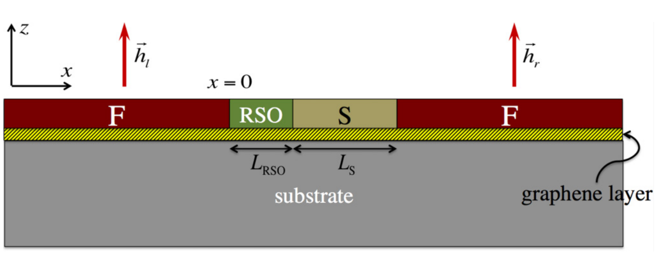

FIG. 1. Schematic of the graphene-based F-RSO-S-F hybrid. The system resides in the xy plane and the junctions are located along the x axis. The length of the RSO and S regions are denoted by $L_{\rm RSO}$ and $L_{\rm S}$. The magnetization of the F regions ($\vec{h}_{l,r}$) are assumed fixed along the z axis. We assume that the ferromagnetism, spin-orbit coupling, and superconductivity is induced into the graphene layer by means of the proximity effect.

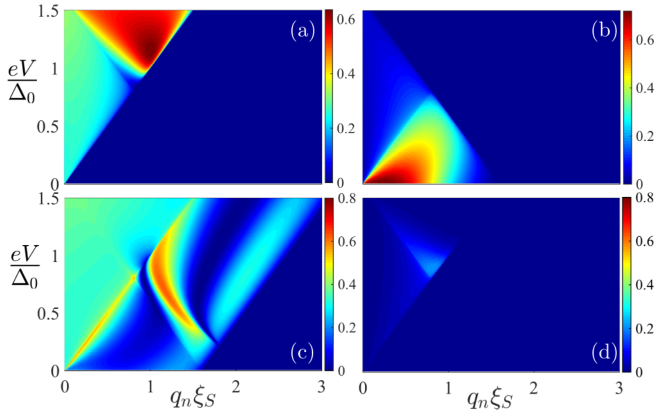

FIG. 2. (a) Spin-reversed cotunneling probability $|t_e^{\downarrow}|^2$. (b) Anomalous crossed Andreev reflection probability $|t_h^{\uparrow}|^2$. (c) Conventional cotunneling $|t_e^{\uparrow}|^2$. (d) Usual CAR $|t_h^{\downarrow}|^2$. The probabilities are plotted vs the transverse component of wave vector q_n and voltage bias across the junction eV. We set $\mu^{\mathrm{F}_l} = \mu^{\mathrm{F}_r} = h_l = h_r = 0.8\Delta_0$, $\mu^{\mathrm{RSO}} = 2.6\Delta_0$, $\lambda = \Delta_0$, $L_{\mathrm{RSO}} = 0.5\xi_S$, $L_{\mathrm{S}} = 0.4\xi_S$.

$\lambda = 1.03$ meV, respectively [56,57], and $L_{\mathrm{S}} = 4$ nm, $L_{\mathrm{RSO}} = 5$ nm. We see that the anomalous CAR has a finite amplitude and its maximum is well isolated from the other transmission channels in the parameter space. Therefore, by tuning the local Fermi levels the system can reside in a regime that allows for a strong signal of the anomalous CAR. According to Fig. 2 this regime is accessible at low voltages $eV \ll \Delta_0$.

The eigenvalues, Eqs. (3), determine the propagation critical angles of moving particles through the junction. By considering the conservation of transverse component of wave vector throughout the system, we obtain the following critical angles [59]:

$$\alpha^c_{e,\downarrow} = \arcsin\left|\frac{\varepsilon + \mu^{F_r} - h_r}{\varepsilon + \mu^{F_l} + h_l}\right|, \tag{6a}$$

$$\alpha^c_{h,\downarrow} = \arcsin\left|\frac{\varepsilon - \mu^{F_r} + h_r}{\varepsilon + \mu^{F_l} + h_l}\right|, \tag{6b}$$

$$\alpha^c_{e,\uparrow} = \arcsin\left|\frac{\varepsilon + \mu^{F_r} + h_r}{\varepsilon + \mu^{F_l} + h_l}\right|, \tag{6c}$$

$$\alpha^c_{h,\uparrow} = \arcsin\left|\frac{\varepsilon - \mu^{F_r} - h_r}{\varepsilon + \mu^{F_l} + h_l}\right|. \tag{6d}$$

These critical angles are useful in calibrating the device properly for a regime of interest. For the spin-reversed cotunneling, the critical angle is denoted by $\alpha^c_{e,\downarrow}$, while for the conventional CAR we show this quantity by $\alpha^c_{h,\downarrow}$. Hence, to filter out these two transmission channels, we set $\mu^{F_r} = h_r$ and choose a representative value $0.8\Delta_0$. In this regime, we see that $\alpha^c_{e(h),\downarrow} \to 0$ at low energies, i.e., $\mu^{F_r}, h_r, \Delta \gg \varepsilon \to 0$ and thus, the corresponding transmissions are eliminated. This is clearly seen in Figs. 2(a) and 2(d) at $eV \ll \Delta_0$. At the same time, the critical angles to the propagation of conventional electron cotunneling and anomalous crossed Andreev reflection reach near their maximum values $\alpha^c_{e(h),\uparrow} \to \pi/2$ consistent with Figs. 2(b) and 2(c). We have analyzed the reflection and transmission processes using a band-structure plot, presented in Ref. [63], that can provide more sense on how a particle is scattered in this regime.

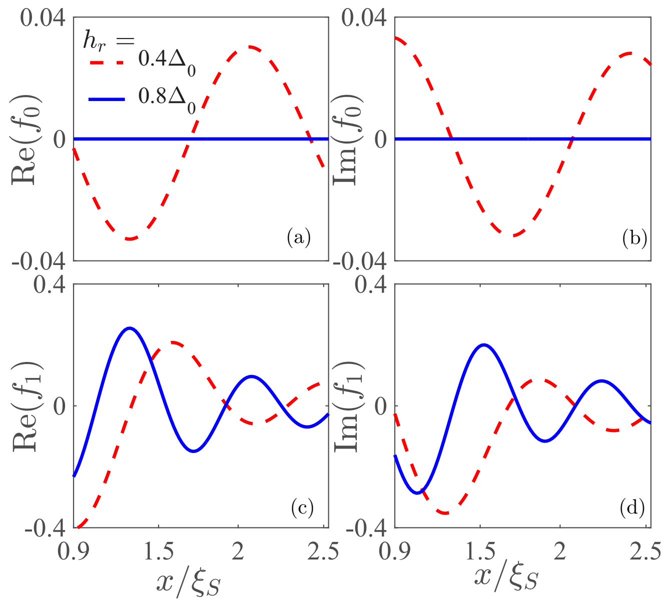

FIG. 3. (a)–(d) Real and imaginary parts of opposite spin f_0 and equal spin pairings f_1 within the F_r region $x \geqslant L_{\mathrm{RSO}} + L_{\mathrm{S}}$ at weak voltages $eV \ll \Delta_0$. The parameter values are the same as those of Fig. 2 except we now compare two cases where $\mu^{F_l} = \mu^{F_r} = h_l = 0.8\Delta_0$ and $h_r = 0.4\Delta_0, 0.8\Delta_0$.

To gain better insights into the anomalous CAR, we calculate the opposite (f_0) and equal (f_1) spin-pair correlations in the F_r region [31,34]:

$$f_0(x,t) = +\frac{1}{2}\sum_{\beta}\xi(t)[u^{\uparrow}_{\beta,K}v^{\downarrow,*}_{\beta,K'} + u^{\uparrow}_{\beta,K'}v^{\downarrow *}_{\beta,K} - u^{\downarrow}_{\beta,K}v^{\uparrow *}_{\beta,K'} - u^{\downarrow}_{\beta,K'}v^{\uparrow *}_{\beta,K}], \tag{7a}$$

$$f_1(x,t) = -\frac{1}{2}\sum_{\beta}\xi(t)[u^{\uparrow}_{\beta,K}v^{\uparrow,*}_{\beta,K'} + u^{\uparrow}_{\beta,K'}v^{\uparrow *}_{\beta,K} + u^{\downarrow}_{\beta,K}v^{\downarrow *}_{\beta,K'} + u^{\downarrow}_{\beta,K'}v^{\downarrow *}_{\beta,K}], \tag{7b}$$

where K and K' denote different valleys and β stands for A and B sublattices [34,59]. Here, $\xi(t) = \cos(\varepsilon t) - i\,\sin(\varepsilon t)\tanh(\varepsilon/2T)$, t is the relative time in the Heisenberg picture, and T is the temperature of the system [31,34]. Figure 3 shows the real and imaginary parts of opposite and equal spin pairings in the F_r region, extended from $x = L_{\mathrm{RSO}} + L_{\mathrm{S}}$ to infinity, at $eV \ll \Delta_0$. For the set of parameters corresponding to Fig. 2, we see that f_0 pair correlation is vanishingly small, while the equal spin triplet pair correlation f_1 has a finite amplitude. We also plot these correlations for a different set of parameters where $\mu^{F_l} = \mu^{F_r} = h_l = 0.8\Delta_0$, while $h_r = 0.4\Delta_0$. The opposite spin triplet pairing f_0 is now nonzero too. Therefore, at low voltages and the parameter set of Fig. 2, the nonvanishing triplet correlation is f_1, which demonstrates the direct link of f_1 and $t_h^{\uparrow}$. This direct connection can be proven by looking at the total wave function in the right

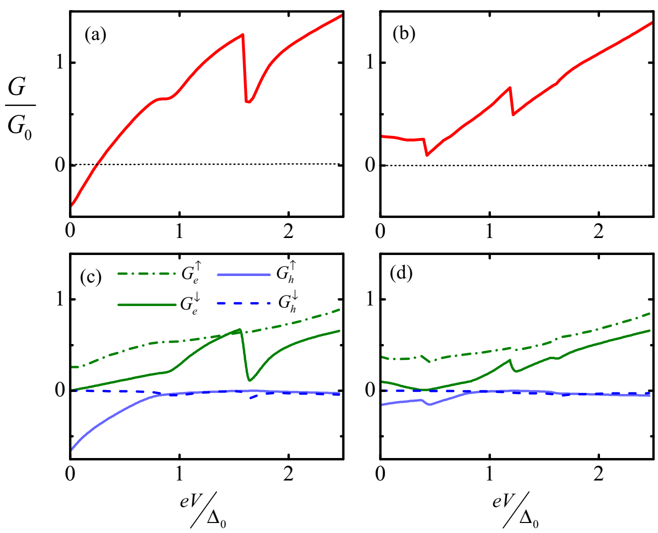

FIG. 4. Charge conductance (top panels) and its components (bottom panels). (a) and (c) charge conductance associated with the probabilities presented in Figs. 2 and 3 ($h_r = 0.8\Delta_0$) and its components, respectively. (b) and (d) the same as panels (a) and (c) except we now consider $h_r = 0.4$ (see Fig. 3). The conductance is normalized by $G_0 = G_\uparrow + G_\downarrow$.

F region, Eq. (5), transmission probabilities shown in Fig. 2, and the definition of triplet correlations, Eqs. (7). One can show that when $t_e^\downarrow$ and $t_h^\downarrow$ vanish, f_0 disappears and f_1 remains nonzero, which offers a spin triplet valve effect.

We calculate the charge conductance through the BTK formalism:

$$G = \int dq_n \sum_{s=\uparrow,\downarrow} G_s\left(\left|t_e^s\right|^2 - \left|t_h^s\right|^2\right), \tag{8}$$

where we define $G_{\uparrow\downarrow} = 2e^2|\varepsilon + \mu_l \pm h_l|W/h\pi$ in which W is the width of the junction. Figures 4(a) and 4(b) exhibit the charge conductance as a function of bias voltage eV across the junction at $h_r = 0.8\Delta_0$ and $0.4\Delta_0$, while the other parameters are set the same as those of Figs. 2 and 3. As seen, the charge conductance is negative at low voltages when $h_r = 0.8\Delta_0$, whereas this quantity becomes positive for $h_r = 0.4\Delta_0$. To gain better insights, we separate the charge conductance into $G_{e,(h)}^{\uparrow\downarrow(\uparrow\downarrow)}$, corresponding to the transmission coefficients $t_{e,(h)}^{\uparrow\downarrow(\uparrow\downarrow)}$ used in Eq. (8). Figures 4(c) and 4(d) illustrate the contribution of different transmission coefficients into the conductance. We see in Fig. 4(c) that $G_h^\uparrow$ dominates the other components and makes the conductance negative. As discussed earlier, this component corresponds to the anomalous CAR which is linked to the equal spin triplet pairing, Fig. 3. This component, however, suppresses when $h_r = 0.4\Delta_0$ so that the other contributions dominate, and therefore the conductance is positive for all energies. Hence, the nonlocal anomalous Andreev reflection found in this work can be revealed in a charge conductance spectroscopy. There are also abrupt changes in the conductance curves that can be fully understood by analyzing the band structure. We present such an analysis in Ref. [63].

In line with the theoretical works summarized in Ref. [59], we have neglected spin-dependent and -independent impurities and disorders as well as substrate and interface effects in our calculations [64–66]. Nonetheless, a recent experiment has shown that such a regime is accessible with today's equipment [62]. Moreover, the same assumptions have already resulted in fundamentally important predictions such as the specular Andreev reflection [59] that was recently observed in experiment [61]. The experimentally measured mean free path of moving particles in a monolayer graphene deposited on top of a hexagonal boron nitride substrate is around $\ell \sim 140$ nm [67]. The coherence length of induced superconductivity into a monolayer graphene using a Nb superconductor was reported as $\xi_S \sim 10$ nm [62]. In this situation, where $\ell \gg \xi_S$, the Andreev mechanism is experimentally relevant. On the other hand, it has been demonstrated that the equal-spin pairings discussed here are long range and can survive even in systems with numerous strong spin-independent scattering resources [40–42]. Therefore, as far as the Andreev mechanism is a relevant scenario in a graphene-based F-RSO-S-F device containing spin-independent scattering resources, i.e., $\ell \gg \xi_S$, we expect that the negative conductance explored in this Rapid Communication is experimentally accessible.

In conclusion, motivated by recent experimental achievements in the induction of spin-orbit coupling into a graphene layer [56,57], we have theoretically studied quantum transport properties of a graphene-based ferromagnet-RSOC-superconductor-ferromagnet junction. Our results reveal that by manipulating the Fermi level in each segment, one can create a dominated anomalous crossed Andreev reflection. We calculate the charge conductance of the system in this regime and show that this phenomenon results in negative charge conductance at low voltages. By calculating various pairing correlations, we demonstrate a direct link between the appearance of anomalous CAR and equal spin triplet correlations. Our findings suggest that a conductance spectroscopy of such a junction can detect the signatures of the anomalous CAR and entanglement of equal spin superconducting triplet pairings in hybrid structures.

Acknowledgments. We are grateful to M. Salehi for valuable and helpful discussions. M.A. also thanks K. Halterman for useful conversations. M.A. is supported by Iran's National Elites Foundation (INEF).

[1] D. Pekker and C. M. Varma, Amplitude/Higgs modes in condensed matter physics, Ann. Rev. Condens. Matter **6**, 269 (2015).

[2] C. W. J. Beenakker, Search for Majorana fermions in superconductors, Ann. Rev. Condens. Matter **4**, 113 (2013).

[3] C. Nayak, S. H. Simon, A. Stern, M. Freedman, and S. Das Sarma, Non-Abelian anyons and topological quantum computation, Rev. Mod. Phys. **80**, 1083 (2008).

[4] M. Eschrig, Spin-polarized supercurrents for spintronics: A review of current progress, Rep. Prog. Phys. **78**, 104501 (2015).

[5] A. Aspect, J. Dalibard, and G. Roger, Experimental Test of Bell's Inequalities Using Time-Varying Analyzers, Phys. Rev. Lett. **49**, 1804 (1982).

[6] A. Steane, Quantum computing, Rep. Prog. Phys. **61**, 117 (1998).

[7] G. B. Lesovik, Th. Martin, and G. Blatter, Electronic entanglement in the vicinity of a superconductor, Eur. Phys. J. B **24**, 287 (2001).

[8] J. M. Raimond, M. Brune, and S. Haroche, Manipulating quantum entanglement with atoms and photons in a cavity, Rev. Mod. Phys. **73**, 565 (2001).

[9] J. Bardeen, L. N. Cooper, and J. R. Schrieffer, Theory of Superconductivity, Phys. Rev. **108**, 1175 (1957).

[10] J. M. Byers and M. E. Flatte, Probing Spatial Correlations with Nanoscale Two-Contact Tunneling, Phys. Rev. Lett. **74**, 306 (1995).

[11] G. Deutscher and D. Feinberg, Coupling superconducting-ferromagnetic point contacts by Andreev reflections, Appl. Phys. Lett. **76**, 487 (2000).

[12] P. Recher, E. V. Sukhorukov, and D. Loss, Andreev tunneling, Coulomb blockade, and resonant transport of nonlocal spin-entangled electrons, Phys. Rev. B **63**, 165314 (2001).

[13] D. Beckmann, H. B. Weber, and H. Lhneysen, Evidence for Crossed Andreev Reflection in Superconductor-Ferromagnet Hybrid Structures, Phys. Rev. Lett. **93**, 197003 (2004).

[14] L. Hofstetter, S. Csonka, J. Nygard, and C. Schonenberger, Cooper pair splitter realized in a two-quantum-dot Y-junction, Nature (London) **461**, 960 (2009).

[15] L. G. Herrmann, F. Portier, P. Roche, A. Levy Yeyati, T. Kontos, and C. Strunk, Carbon Nanotubes as Cooper-Pair Beam Splitters, Phys. Rev. Lett. **104**, 026801 (2010).

[16] L. Hofstetter, S. Csonka, A. Baumgartner, G. Fülöp, S. d'Hollosy, J. Nygård, and C. Schönenberger, Finite-Bias Cooper Pair Splitting, Phys. Rev. Lett. **107**, 136801 (2011).

[17] G. Fülöp, S. d'Hollosy, A. Baumgartner, P. Makk, V. A. Guzenko, M. H. Madsen, J. Nygård, C. Schönenberger, and S. Csonka, Local electrical tuning of the nonlocal signals in a Cooper pair splitter, Phys. Rev. B **90**, 235412 (2014).

[18] N. M. Chtchelkatchev and I. S. Burmistrov, Andreev conductance of a domain wall, Phys. Rev. B **68**, 140501(R) (2003).

[19] M. S. Kalenkov and A. D. Zaikin, Nonlocal Andreev reflection at high transmissions, Phys. Rev. B **75**, 172503 (2007).

[20] G. Bignon, M. Houzet, F. Pistolesi, and F. W. J. Hekking, Current-current correlations in hybrid superconducting and normal-metal multiterminal structures, Europhys. Lett. **67**, 110 (2004); R. Mlin, C. Benjamin, and T. Martin, Positive cross correlations of noise in superconducting hybrid structures: Roles of interfaces and interactions, Phys. Rev. B. **77**, 094512 (2008).

[21] E. Amitai, R. P. Tiwari, S. Walter, T. L. Schmidt, and S. E. Nigg, Nonlocal quantum state engineering with the Cooper pair splitter beyond the Coulomb blockade regime, Phys. Rev. B **93**, 075421 (2015).

[22] S. Walter, J. C. Budich, J. Eisert, and B. Trauzettel, Entanglement of nanoelectromechanical oscillators by Cooper-pair tunneling, Phys. Rev. B **88**, 035441 (2013).

[23] H. Cheraghchi, H. Esmailzadeh, and A. G. Moghaddam, Superconducting electron and hole lenses, Phys. Rev. B **93**, 214508 (2016).

[24] G. C. Paul and A. Saha, Quantum charge pumping through resonant crossed Andreev reflection in superconducting hybrid junction of silicene, Phys. Rev. B **95**, 045420 (2017).

[25] R. Hussein, L. Jaurigue, M. Governale, and A. Braggio, Double quantum dot Cooper-pair splitter at finite couplings, Phys. Rev. B **94**, 235134 (2016).

[26] J. Cayssol, Crossed Andreev Reflection in a Graphene Bipolar Transistor, Phys. Rev. Lett. **100**, 147001 (2008).

[27] J. Linder, M. Zareyan, and A. Sudb, Spin-switch effect from crossed Andreev reflection in superconducting graphene spin valves, Phys. Rev. B **80**, 014513 (2009).

[28] A. I. Buzdin, Proximity effects in superconductor-ferromagnet heterostructures, Rev. Mod. Phys. **77**, 935 (2005).

[29] F. S. Bergeret, A. F. Volkov, and K. B. Efetov, Odd triplet superconductivity and related phenomena in superconductor-ferromagnet structures, Rev. Mod. Phys. **77**, 1321 (2005).

[30] R. S. Keizer, S. T. B. Goennenwein, T. M. Klapwijk, G. Miao, G. Xiao, and A. Gupta, A spin triplet supercurrent through the half-metallic ferromagnet CrO_2, Nature (London) **439**, 825 (2006).

[31] K. Halterman, P. H. Barsic, and O. T. Valls, Odd Triplet Pairing in Clean Superconductor/Ferromagnet Heterostructures, Phys. Rev. Lett. **99**, 127002 (2007).

[32] M. G. Blamire and J. W. A. Robinson, The interface between superconductivity and magnetism: Understanding and device prospects, J. Phys.: Condens. Matter **26**, 453201 (2014).

[33] Y. N. Khaydukov, G. A. Ovsyannikov, A. E. Sheyerman, K. Y. Constantinian, L. Mustafa, T. Keller, M. A. Uribe-Laverde, Yu. V. Kislinskii, A. V. Shadrin, A. Kalabukhov, B. Keimer, and D. Winkler, Evidence for spin-triplet superconducting correlations in metal-oxide heterostructures with noncollinear magnetization, Phys. Rev. B **90**, 035130 (2014).

[34] K. Halterman, O. T. Valls, and M. Alidoust, Spin-Controlled Superconductivity and Tunable Triplet Correlations in Graphene Nanostructures, Phys. Rev. Lett. **111**, 046602 (2013).

[35] A. Moor, A. F. Volkov, and K. B. Efetov, Nematic versus ferromagnetic spin filtering of triplet Cooper pairs in superconducting spintronics, Phys. Rev. B **92**, 180506(R) (2015).

[36] J. W. A. Robinson, J. D. S. Witt, and M. G. Blamire, Controlled injection of spin-triplet supercurrents into a strong ferromagnet, Science **329**, 59 (2010).

[37] M. Alidoust and J. Linder, Spin-triplet supercurrent through inhomogeneous ferromagnetic trilayers, Phys. Rev. B **82**, 224504 (2010).

[38] T. E. Baker, A. Richie-Halford, and A. Bill, Long range triplet Josephson current and 0π transition in tunable domain walls, New J. Phys. **16**, 093048 (2014).

[39] M. G. Flokstra, N. Satchell, J. Kim, G. Burnell, P. J. Curran, S. J. Bending, J. F. K. Cooper, C. J. Kinane, S. Langridge, A. Isidori, N. Pugach, M. Eschrig, H. Luetkens, A. Suter, T. Prokscha, and S. L. Lee, Remotely induced magnetism in a normal metal using a superconducting spin-valve, Nat. Phys. **12**, 57 (2016).

[40] F. S. Bergeret and I. V. Tokatly, Spin-orbit coupling as a source of long-range triplet proximity effect in superconductor-ferromagnet hybrid structures, Phys. Rev. B **89**, 134517 (2014).

[41] M. Alidoust and K. Halterman, Spontaneous edge accumulation of spin currents in finite-size two-dimensional diffusive spin-orbit coupled SFS heterostructures, New J. Phys. **17**, 033001 (2015).

[42] M. Alidoust and K. Halterman, Long-range spin-triplet correlations and edge spin currents in diffusive spin-orbit coupled SNS

hybrids with a single spin-active interface, J. Phys.: Condens. Matter **27**, 235301 (2015).

[43] Ya. V. Fominov, A. A. Golubov, and M. Yu. Kupriyanov, Superconducting triplet spin valve, JETP Lett. **77**, 510 (2003).

[44] A. Srivastava, L. A. B. Olde Olthof, A. Di Bernardo, S. Komori, M. Amado, C. Palomares-Garcia, M. Alidoust, K. Halterman, M. G. Blamire, and J. W. A. Robinsonn, Magnetization-control and transfer of spin-polarized Cooper pairs into a half-metal manganite, arXiv:1706.00332.

[45] A. Singh, S. Voltan, K. Lahabi, and J. Aarts, Colossal Proximity Effect in a Superconducting Triplet Spin Valve Based on the Half-Metallic Ferromagnet CrO_2, Phys. Rev. X **5**, 021019 (2015).

[46] K. Halterman and M. Alidoust, Half-metallic superconducting triplet spin valve, Phys. Rev. B **94**, 064503 (2016).

[47] Y. Kalcheim, O. Millo, A. Di Bernardo, A. Pal, and J. W. A. Robinson, Inverse proximity effect at superconductor-ferromagnet interfaces: Evidence for induced triplet pairing in the superconductor, Phys. Rev. B **92**, 060501(R) (2015).

[48] M. Alidoust, K. Halterman, and O. T. Valls, Zero energy peak and triplet correlations in nanoscale SFF spin valves, Phys. Rev. B **92**, 014508 (2015).

[49] M. Alidoust, A. Zyuzin, and K. Halterman, Pure odd-frequency superconductivity at the cores of proximity vortices, Phys. Rev. B **95**, 045115 (2017).

[50] L. Kuerten, C. Richter, N. Mohanta, T. Kopp, A. Kampf, J. Mannhart, and H. Boschker, In-gap states in superconducting $LaAlO_3$–$SrTiO_3$ interfaces observed by tunneling spectroscopy, Phys. Rev. B **96**, 014513 (2017).

[51] C. Visani, Z. Sefrioui, J. Tornos, C. Leon, J. Briatico, M. Bibes, A. Barthelemy, J. Santamaria, and Javier E. Villegas, Equal-spin Andreev reflection and long-range coherent transport in high-temperature superconductor/half-metallic ferromagnet junctions, Nat. Phys. **8**, 539 (2012).

[52] S. Matsuo, K. Ueda, S. Baba, H. Kamata, M. Tateno, J. Shabani, C. J. Palmstrm, and S. Tarucha, Equal-spin Andreev reflection in junctions of spin-resolved quantum Hall bulk state and spin-singlet superconductor, arXiv:1703.03189.

[53] R. Beiranvand, H. Hamzehpour, and M. Alidoust, Tunable anomalous Andreev reflection and triplet pairings in spin-orbit-coupled graphene, Phys. Rev. B **94**, 125415 (2016).

[54] M. M. Maska and T. Domanski, Spin-polarized Andreev tunneling through the Rashba chain, arXiv:1706.01468.

[55] Z.-M. Yu, Y. Liu, Y. Yao, and S. A. Yang, Unconventional pairing induced anomalous transverse shift in Andreev reflection, arXiv:1708.06915.

[56] A. Avsar, J. Y. Tan, T. Taychatanapat, J. Balakrishnan, G. K. W. Koon, Y. Yeo, J. Lahiri, A. Carvalho, A. S. Rodin, E. C. T. OFarrell, G. Eda, A. H. Castro Neto, and B. Ozyilmaz, Spin–orbit proximity effect in graphene, Nat. Commun. **5**, 4875 (2014).

[57] Z. Wang, C. Tang, R. Sachs, Y. Barlas, and J. Shi, Proximity-Induced Ferromagnetism in Graphene Revealed by the Anomalous Hall Effect, Phys. Rev. Lett. **114**, 016603 (2015).

[58] H. B. Heersche, P. Jarillo-Herrero, J. B. Oostinga, L. M. K. Vandersypen, and A. F. Morpurgo, Bipolar supercurrent in graphene, Nature (London) **446**, 56 (2006).

[59] C. W. J. Beenakker, *Colloquium:* Andreev reflection and Klein tunneling in graphene, Rev. Mod. Phys. **80**, 1337 (2008).

[60] K. Halterman, O. T. Valls, and M. Alidoust, Characteristic energies, transition temperatures, and switching effects in clean S|N|S graphene nanostructures, Phys. Rev. B **84**, 064509 (2011).

[61] D. K. Efetov, L. Wang, C. Handschin, K. B. Efetov, J. Shuang, R. Cava, T. Taniguchi, K. Watanabe, J. Hone, C. R. Dean, and P. Kim, Specular interband Andreev reflections at van der Waals interfaces between graphene and $NbSe_2$, Nat. Phys. **12**, 328 (2016).

[62] M. Ben Shalom, M. J. Zhu, V. I. Fal'ko, A. Mishchenko, A. V. Kretinin, K. S. Novoselov, C. R. Woods, K. Watanabe, T. Taniguchi, A. K. Geim, and J. R. Prance, Quantum oscillations of the critical current and high-field superconducting proximity in ballistic graphene, Nat. Phys. **12**, 318 (2016).

[63] See Supplemental Material at http://link.aps.org/supplemental/10.1103/PhysRevB.96.161403 for more details of calculations and analyses.

[64] C. Ertler, S. Konschuh, M. Gmitra, and J. Fabian, Electron spin relaxation in graphene: The role of the substrate, Phys. Rev. B **80**, 041405(R) (2009).

[65] V. K. Dugaev, E. Ya. Sherman, and J. Barnas, Spin dephasing and pumping in graphene due to random spin-orbit interaction, Phys. Rev. B **83**, 085306 (2011).

[66] I. M. Vicent, H. Ochoa, and F. Guinea, Spin relaxation in corrugated graphene, Phys. Rev. B **95**, 195402 (2017).

[67] L. Bretheau, J. Wang, R. Pisoni, K. Watanabe, T. Taniguchi, and P. Jarillo-Herrero, Tunnelling spectroscopy of Andreev states in graphene, Nat. Phys. **13**, 756 (2017).